Available online at www.sciencedirect.com
ScienceDirect
Trans. Nonferrous Met. Soc. China 35(2025) 257−270
Transactions of Nonferrous Metals Society of China
www.tnmsc.cn

Efficient chemical mechanical polishing of W promoted by Fenton-like reaction between Cu^{2+} and H_2O_2

Hong-yu CHEN[1,2], Lin WANG[1], Feng PENG[1], Meng-meng SHEN[1], Wei HANG[1,2], Tufa Habtamu BERI[3], Hui-bin ZHANG[4], Jun ZHAO[1,2], Yun-xiao HAN[1,2], Bing-hai LÜ[1,2]

1. College of Mechanical Engineering, Zhejiang University of Technology, Hangzhou 310023, China;
2. Key Laboratory of Special Purpose Equipment and Advanced Processing Technology, Ministry of Education, Zhejiang University of Technology, Hangzhou 310023, China;
3. Adama Science and Technology University, Adama 1888, Ethiopia;
4. College of Materials Science and Engineering, Zhejiang University of Technology, Hangzhou 310014, China

Received 16 May 2023; accepted 26 December 2023

Abstract: The Fenton-like reaction between Cu^{2+} and H_2O_2 was employed in chemical mechanical polishing to achieve efficient and high-quality processing of tungsten. The microstructure evolution and material removal rate of tungsten during polishing process were investigated via scanning electron microscopy, X-ray photoelectron spectroscopy, ultraviolet−visible spectrophotometry, and electrochemical experiments. The passivation behavior and material removal mechanism were discussed. Results show that the use of mixed H_2O_2+$Cu(NO_3)_2$ oxidant can achieve higher polishing efficiency and surface quality compared with the single oxidant $Cu(NO_3)_2$ or H_2O_2. The increase in material removal rate is attributed to the rapid oxidation of W into WO_3 via the chemical reaction between the substrate and hydroxyl radicals produced by the Fenton-like reaction. In addition, material removal rate and static etch rate exhibit significantly different dependencies on the concentration of $Cu(NO_3)_2$, while the superior oxidant for achieving the balance between polishing efficiency and surface quality is 0.5 wt.% H_2O_2 +1.0 wt.% $Cu(NO_3)_2$.

Key words: chemical mechanical polishing; tungsten; Fenton-like reaction; hydroxyl radical; material removal mechanism

1 Introduction

Currently, tungsten (W) is widely used in high-tech fields, such as national defense, aerospace, integrated circuits, and nuclear reactors, due to its excellent physical properties like high melting point, high thermal conductivity, low thermal expansion coefficient, high corrosion resistance, and high sputtering resistance [1−3]. However, the inherent disadvantages of the material, such as hard brittle characteristics and high chemical stability, limit the processing efficiency and application of W [4−6]. Traditional processing techniques inevitably result in high residual stress on the surface, subsequently leading to the formation of subsurface cracks and brittle fractures [7]. Ultra-precision polishing serves as the final step in the surface processing chain, aiming to eliminate defects such as surface damage induced by prior processes, diminish product surface roughness, and attain exceptional processing quality.

XU et al [8] evaluated different polishing methods for W and proposed chemical mechanical

Corresponding author: Wei HANG, Tel: +86-15988109849, E-mail: whang@zjut.edu.cn;
Hui-bin ZHANG, Tel: +86-15168442898, E-mail: zhanghb@zjut.edu.cn
https://doi.org/10.1016/S1003-6326(24)66678-1

polishing (CMP) as the current mainstream polishing method due to its high efficiency and cost-effectiveness. The mechanism of tungsten chemical mechanical polishing (W-CMP) in the planarization process includes two steps. The first step is to form a soft tungsten oxide passivation layer on the W surface by continuously supplying oxidants. In the second step, this passivation layer is continuously removed by mechanical wear. And actually, the above two steps are carried out simultaneously [9]. In the process of actual polishing, the rapid and efficient formation of a surface oxide layer plays a pivotal role in achieving a high removal rate and exceptional polishing performance. Consequently, the identification of a suitable oxidant holds paramount importance [10,11]. Single or composite abrasives, such as silica (SiO_2), alumina (Al_2O_3), cerium oxide (CeO_2), and diamond, along with various oxidants like hydrogen peroxide (H_2O_2), ferric nitrate ($Fe(NO_3)_3$), potassium permanganate ($KMnO_4$), potassium iodate (KIO_3), and potassium ferricyanide ($K_3Fe(CN)_6$), have been used in W-CMP processes [12]. Indeed, experiments have shown that the W surface fails to achieve complete planarization and optimal polishing efficiency when using a single oxidant due to the poor passivation effect during the CMP process [13,14].

Another method proposed by many researchers is to combine different catalysts with H_2O_2 to increase the polishing rate of W by enhancing the converting rate of passivation layer [15]. PODDAR et al [16] added FeSi as a nano-catalyst into the acidic polishing solution with H_2O_2 as oxidant for CMP of W. This method notably reduced the metal ion pollution on the surface, but the enhancement in polishing rate was not significantly apparent. LIM et al [17] reported an increased W polishing rate due to the rapid formation of WO_x in the presence of in-situ generated strong oxidizing substances produced in catalytic reaction of ferri ions (Fe^{3+}) to H_2O_2. LIM et al [18] also investigated the catalytic effect of $Fe(NO_3)_3$ at different concentrations during the W-CMP process. It was found that the W polishing rate varies obviously with the concentration of $Fe(NO_3)_3$. In another study, ZHOU et al [19] found that the conventional Fenton reaction using Fe^{3+} to catalyze the decomposition of H_2O_2 to form hydroxyl radicals (·OH) was limited in a narrow working pH range (pH=2−4), which posed an obstacle to enhancing the removal efficiency of W using SiO_2 abrasive. Therefore, it is necessary to find a more efficient W-CMP slurry for achieving high polishing rate and satisfied surface quality. Copper ions (Cu^{2+}) are used as catalysts because of their similar redox properties to Fe^{3+}, and the reactivity of Cu^{2+} with H_2O_2 is higher than that of Fe^{3+} [20]. Utilizing the Fenton-like reaction involving Cu^{2+} and H_2O_2 instead of the traditional Fenton reaction can extend the working pH range to neutral or mildly alkaline conditions. So far, the effect of H_2O_2+$Cu(NO_3)_2$ mixed oxidants on the W-CMP mechanism, including the catalytic reaction mechanism, material removal mechanism, surface morphology evolution, and process optimization, has less been reported yet.

In this study, the CMP of W was carried out under weak alkaline conditions with mixed oxidants of H_2O_2+$Cu(NO_3)_2$. To verify the catalytic effect of $Cu(NO_3)_2$, the polishing rates of different slurries containing either single $Cu(NO_3)_2$ or H_2O_2 oxidant were compared with that of mixed oxidants, and the most superior oxidant ratio was determined. This study involved a thorough investigation of the material corrosion and material removal behavior during W-CMP. The resulting findings could provide a reference for efficient and low damage processing of W.

2 Experimental

2.1 Polishing experiments

High-purity W was prepared by powder metallurgy and strengthened by the rolling process. After annealing treatment [21], W samples were machined to 10 mm × 10 mm × 1 mm by wire-electrode cutting. H_2O_2 (30 wt.% solution, Merck, China) and deionized water were mixed in a ratio of 1:1 and heated to boiling to prepare the metallographic sample. The abrasives used in these experiments were colloidal SiO_2 (YZ8040, Macklin, China). H_2O_2 and $Cu(NO_3)_2$ (C860751, Macklin, China) were used as oxidants. The slurries were prepared by selectively adding chemical reagents to deionized water, and the pH was adjusted using $C_6H_8O_7$ (C805019, Microline, China) and KOH (P816399, Microline, China). Real-time pH measurements were conducted using a pH measurement instrument (PB-10, Sartorius, Germany). To prepare different slurries, deionized

water was added to dilute the abrasive to a specified concentration before adding the oxidant. A chemical reagent was then used to maintain the pH at a level of 9. Finally, the oxidant was added and the mixture was thoroughly stirred. The filtered slurry was then obtained for use. Moreover, a desktop polishing machine (UNIPOL-1200S, Kejing, China) and laminated polyurethane pads (IC1300/Suba IV) were used to investigate the characteristics of W-CMP. The specific experimental parameters are given in Table 1.

Table 1 W-CMP experimental parameters

Parameter	Value or description
Polishing pad speed/(r·min^{-1})	80
Workpiece speed/(r·min^{-1})	30
Pressure/kPa	22.923
Abrasive	SiO_2
Polishing pad	Polyurethane
Abrasive concentration/wt.%	4.0
Slurry flow rate/(mL·min^{-1})	70.0
H_2O_2 concentration/wt.%	0, 0.1, 0.5, 1.0, 1.5, 2.0
$Cu(NO_3)_2$ concentration/wt.%	0, 0.1, 0.5, 1.0, 1.5, 2.0
Sample size/mm^3	10×10×1

2.2 Characterization

The calculation formulas for material removal rate (MRR (nm/min)) and static etch rate (SER (nm/min)) are as follows:

$$\text{MRR(or SER)}=\Delta m\cdot(\rho tS)^{-1} \quad (1)$$

where Δm (g) is the mass difference before and after polishing treatment measured by precision balance; ρ (g/cm^3) is the density of W samples; S (cm^2) is the area of the sample; t (min) is the time used to process the sample. SER was obtained by immersing a sample in a base solution at 25 °C for 30 min.

The composition and chemical state of treated W surfaces were estimated by an XPS spectrometer (AXIS Ultra DLD, Kratos, Analytical) and an energy spectrometer (BNXFD 5010, Bruker, Germany). A white light interferometer (Super View W1, Chotest, China) was used to measure the surface roughness and three-dimensional morphology of the processed samples. Each measurement took five different points in the same area, and the scanning range was 20 μm. The surface morphology and microstructure evolution of the samples were investigated by SEM (ΣIGMA, ZEISS, Germany). Electrochemical analysis was performed via a potentiostat (Autolab PGSTAT302 N, Metrohm, Switzerland). During the experiment, the tungsten sample was used as the working electrode. The AgCl and platinum (Pt) were used as the reference electrode and counter electrode, respectively. The voltage scanning rate was set to be 5 mV/s.

The PNDA (N,N-dimethyl-p-nitrosoaniline) (N838515, Macklin, China) was selected as an ·OH trapping agent [22], and the content of ·OH in the slurry was quantitatively detected by an ultraviolet−visible spectrophotometer (UV-2700, Shimadzu, China). A PNDA solution (4.15×10^{-5} mol/L) and the prepared slurry (120 μL) were mixed in a cuvette, which was then placed in an ultraviolet-visible spectrophotometer for measuring absorption intensity. The experiments were repeated three times, and the average values were used for analysis.

3 Results and discussion

3.1 Effect of slurry composition on polishing performance

The metallograph of the rolled W sample is shown in Fig. 1. It is seen that the sintered bulk W is nearly completely dense and the grains present obvious orientation along the rolling direction. Rolled W inevitably has defects such as small residual holes or microcracks.

The schematic diagram for W-CMP is described in Fig. 2. In the presence of oxidants, an oxide passivation layer with low hardness can be formed to improve the abrasive removal efficiency. The polishing pad consists of a porous polyurethane-based polymer sheet and a foam substrate. The polyurethane possesses excellent elasticity, facilitating superior adaptation to changes in the surface morphology during the polishing process. This characteristic ensures the provision of uniform polishing pressure, as illustrated in Fig. 2(b).

By adjusting the pH values of the slurry, the changes in MRR and R_a of W-CMP under various conditions were studied, as shown in Fig. 3. The MRR of W is only 6.206 nm/min at pH=7, but steadily increased to 11.201 nm/min as the pH value

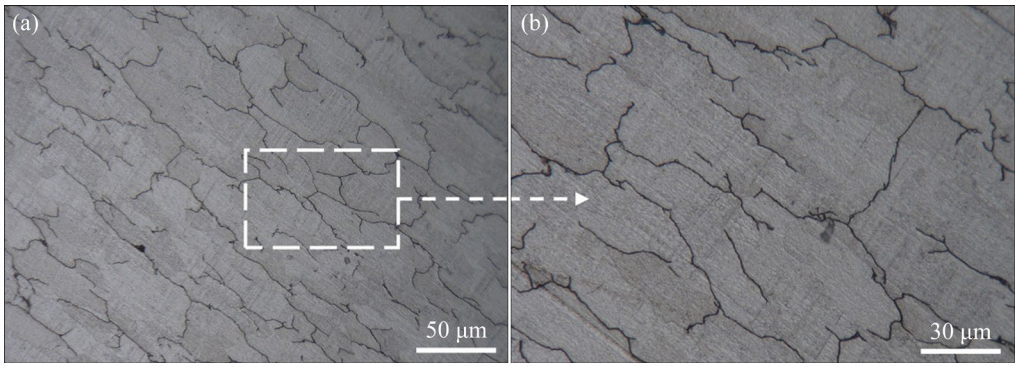

Fig. 1 Microstructure image of W (a) and its local enlarged image (b)

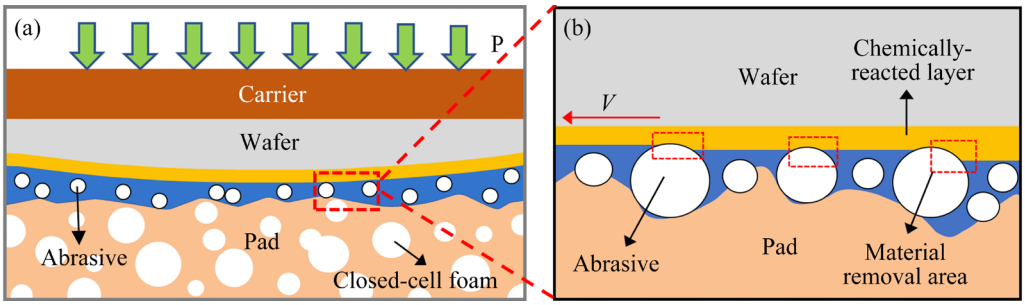

Fig. 2 Process schematic diagram (a) and material removal mechanism (b) of W-CMP

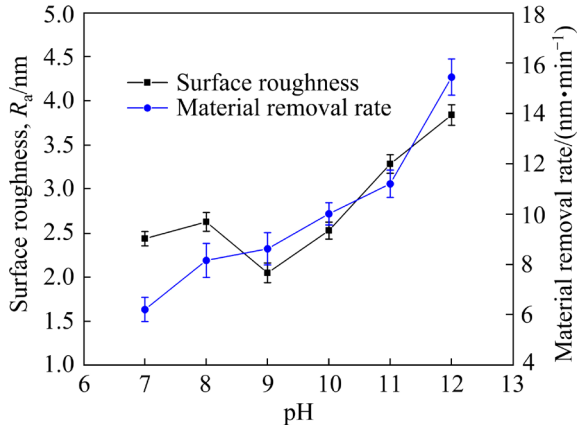

Fig. 3 Changes of R_a and MRR of W-CMP at different pH values

rises to 11. Combined with the morphology of the processed surface of W workpiece in Fig. 4(a), it is found that under neutral conditions, R_a and S_a, two indicators of W surface roughness, are 2.44 and 8.47 nm, respectively. The overall surface morphology is relatively uniform without obvious corrosion. When the pH reaches 9, these two indicators decrease to 2.05 and 6.13 nm, respectively. Corrosion is directly visible in the surface morphology, but it is more uniform than that at pH=8 (Figs. 4(b, c)). With the increase of hydroxide concentration in the slurry, the wear and concave caused by corrosion on the material surface become more obvious (Figs. 4(d, e)). When pH>11, the corrosion morphology of grain boundaries can be clearly observed (Fig. 4(f)). The above result indicates that the increased alkalinity of the slurry facilitates the dissolution of the oxide layer, resulting in the increase of the MRR and the non-uniform corrosion of the W surface.

Figure 5(a) shows the MRR of W-CMP with different oxidants, where the slurry without oxidant is denoted as “R”. It is found that the MRR of W is only 6.511 nm/min before adding oxidants, but increased to 18.088 and 38.118 nm/min after the addition of 1.0 wt.% $Cu(NO_3)_2$ and 0.5 wt.% H_2O_2, respectively. MRR is further enhanced when the mixed oxidants of H_2O_2+$Cu(NO_3)_2$ is used. The highest MRR value of 68.271 nm/min is obtained when the concentrations of H_2O_2 and $Cu(NO_3)_2$ are 0.5 wt.%. With the further progressive increase of $Cu(NO_3)_2$ concentration, MRR first decreases and subsequently rises. The above results show that the addition of the mixed oxidants significantly improves the MRR of W-CMP, while excessive $Cu(NO_3)_2$ is detrimental to the polishing efficiency. A optimal polishing efficiency can be achieved by adding 0.5−1.0 wt.% $Cu(NO_3)_2$ when keeping the H_2O_2 concentration fixed at 0.5 wt.%.

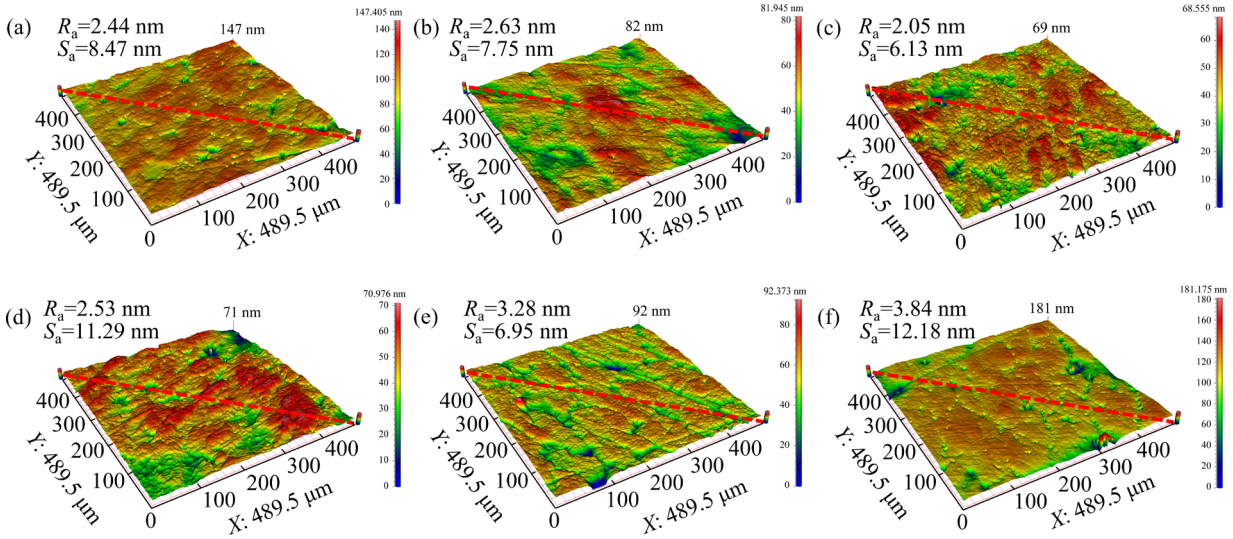

Fig. 4 Three-dimensional surface morphologies of W samples after polishing at different pH values: (a) 7; (b) 8; (c) 9; (d) 10; (e) 11; (f) 12

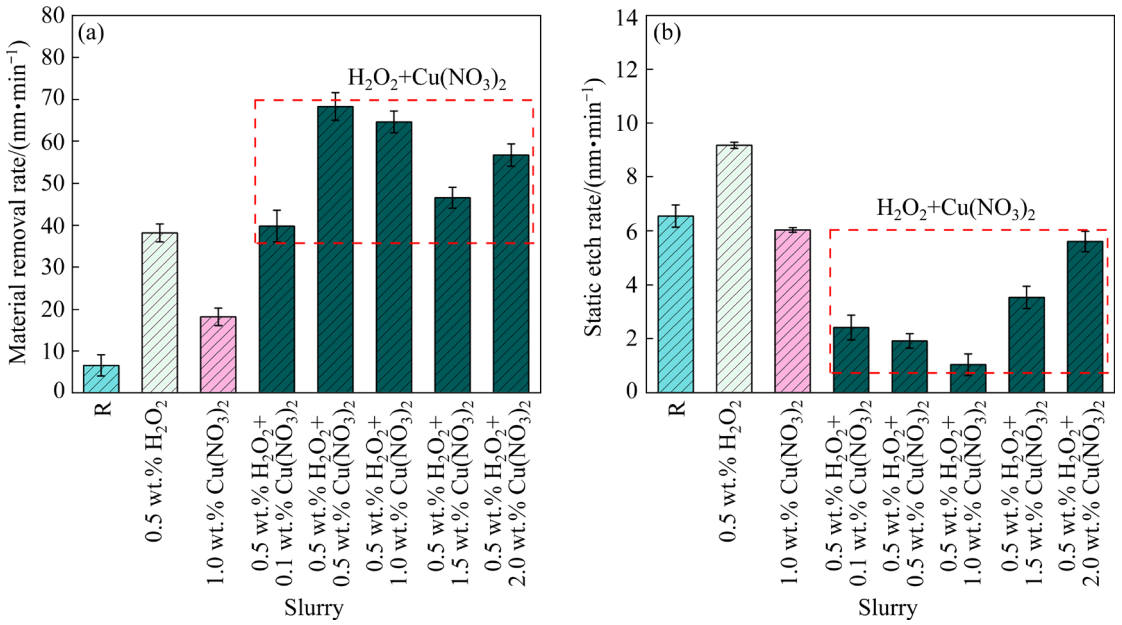

Fig. 5 Changes of MRR (a) and SER (b) in slurries with single and mixed oxidants (R is the slurry without oxidant)

For a deep understanding of the material removal mechanism of W-CMP, W samples were immersed in different slurries for 15 min to calculate SER, as shown in Fig. 5(b). It is seen that the SER values are all larger than 6 nm/min in R and slurries with single 0.5 wt.% H_2O_2 or 1.0 wt.% Cu(NO$_3$)$_2$, but smaller than 6 nm/min in H_2O_2 + Cu(NO$_3$)$_2$ slurries. SER value firstly decreases and subsequently increases with the increasing of Cu(NO$_3$)$_2$ concentration. The minimum of 1.033 nm/min appears when the concentration of Cu(NO$_3$)$_2$ is 1.0 wt.% in the mixed slurries. This tendency is opposite to that of MRR, which highlights the need for further investigation into the specific corrosion and material removal mechanism in combination with surface morphology.

In this study, different oxidant components were added to the slurries for polishing W, and the surface morphologies after CMP were observed. In Fig. 6(a), there is obvious corrosion on the surface after treatment with R slurry, and R_a and S_a are 2.05 and 6.13 nm, respectively. The addition of Cu(NO$_3$)$_2$ only slightly reduces the surface roughness. Contrastively, W surface with an excellent polishing quality is obtained by using mixed oxidants, and its R_a reaches the minimum value of 1.75 nm when the

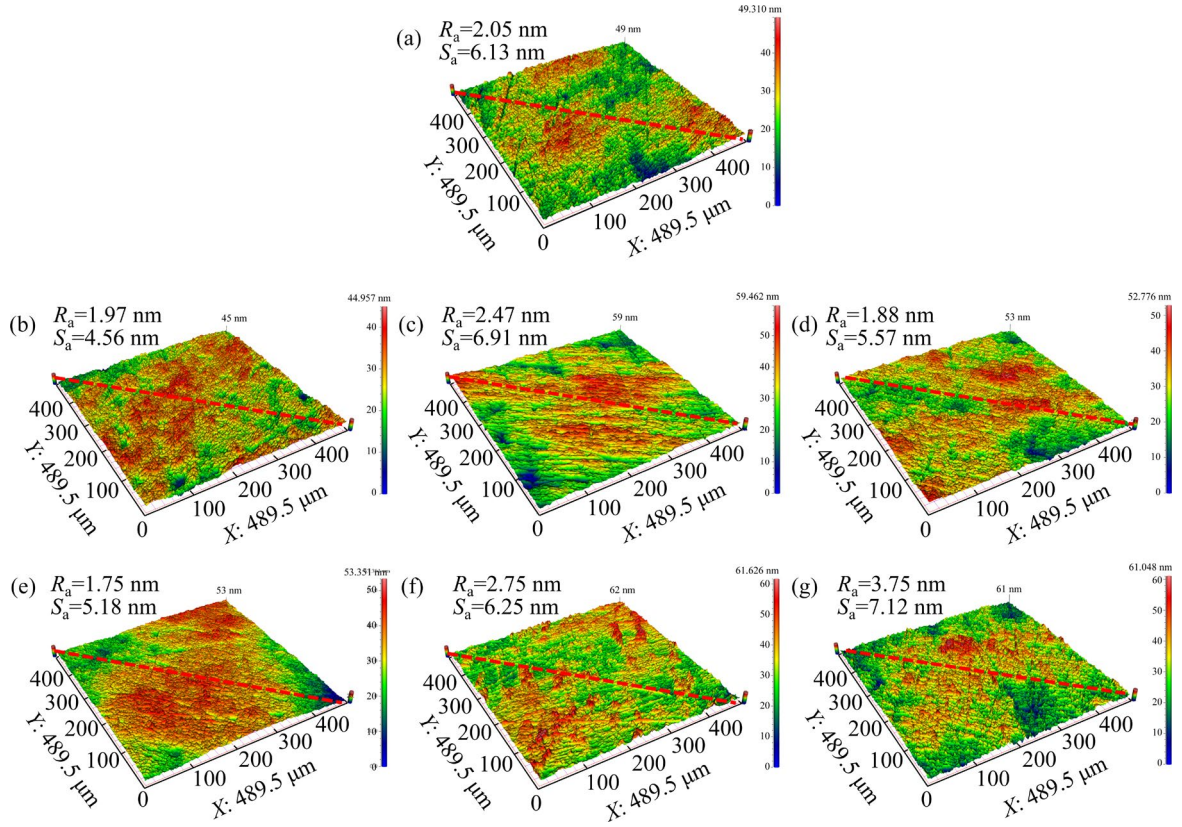

Fig. 6 Three-dimensional surface morphologies of W samples after polishing with different oxidant slurries: (a) R; (b) 1.0 wt.% $Cu(NO_3)_2$; (c) 0.5 wt.% H_2O_2 + 0.1 wt.% $Cu(NO_3)_2$; (d) 0.5 wt.% H_2O_2 + 0.5 wt.% $Cu(NO_3)_2$; (e) 0.5 wt.% H_2O_2 + 1.0 wt.% $Cu(NO_3)_2$; (f) 0.5 wt.% H_2O_2 + 1.5 wt.% $Cu(NO_3)_2$; (g) 0.5 wt.% H_2O_2 + 2.0 wt.% $Cu(NO_3)_2$

concentrations of H_2O_2 and $Cu(NO_3)_2$ are 0.5 wt.% and 1.0 wt.%, respectively. Results demonstrate that a stable tungsten oxide layer is generated on the W surface when using the mixed oxidants, which prevents the slurry corrosion. Additionally, when the concentration of $Cu(NO_3)_2$ in the mixed oxidants exceeds 1.5 wt.%, uniform corrosion of the W surface is observed. This could be attributed to the excessive amount of $Cu(NO_3)_2$ preventing the oxidation of W and increasing the corrosion rate of W surface.

3.2 Passivation behavior of W under Fenton-like effect

The material removal mechanism of W-CMP under the action of a single oxidant was proposed based on MRR, SER, and surface quality. In alkaline conditions, the formation rate of oxide layer on W is slow, and hydroxide ions (OH^-) have a significant corrosive effect on the tungsten oxide layer. This leads to non-uniform corrosion of the micro-convex peaks on the surface of W. These findings align with the results reported by XU et al [23]. The analysis of higher SER and lower MRR indicates that $Cu(NO_3)_2$ is not conducive to the formation of a thick passivation layer on the W surface, which is the main driving force for the removal of W during CMP. In addition, a single reagent of H_2O_2 is commonly used to produce complex tungstate compounds (such as $H_2W_2O_{11}$ and $H_2W_3O_{12}$) to aid in the dissolution of W and promote the formation of a porous oxide layer instead of stable WO_3. The specific reactions proposed by KNEER et al [24] are listed as follows:

$$W+2H_2O_2=WO_2+2H_2O \quad (2)$$

$$WO_2+6H_2O_2=H_2W_2O_{11}+5H_2O \quad (3)$$

$$3H_2W_2O_{11}+7H_2O_2=2H_2W_3O_{12}+8H_2O \quad (4)$$

Initially, W reacts with H_2O_2 to form WO_2. It should be noted that in the case of excessive H_2O_2, WO_2 would be further transformed into a highly soluble $H_2W_3O_{11}$. When H_2O_2 is excessive, the hydrolysis of the peroxide intermediate ($H_2W_3O_{11}$) can be finally converted into $H_2W_3O_{12}$. The presence of $H_2W_3O_{12}$ is unable to further inhibit

the corrosion of W surface, leading to a high SER under the action of H_2O_2. In other words, the formation of $H_2W_2O_{11}$ and $H_2W_3O_{12}$ does not provide effective protection against the corrosive effect of single H_2O_2 oxidant. The compositions of the oxide layers on the treated W surface were analyzed by XPS, as shown in Fig. 7(a). W $4f_{7/2}$ and $4f_{5/2}$ peaks are respectively located at (31.6±0.2) and (33.8±0.2) eV, and W^{6+} $4f_{7/2}$ and $4f_{5/2}$ peaks appear at (35.7±0.2) and (37.8±0.2) eV, respectively. The percentages of each fitted peak areas are shown in Fig. 7(b). It can be seen that there are only trace W^{6+} peaks after treating with R slurry or 1.0 wt.% $Cu(NO_3)_2$ slurry, which indicates that the generating rate of oxide layer is low in this condition. Under the condition of the mixed oxidants of H_2O_2+$Cu(NO_3)_2$, the peak intensity of W^{6+} firstly increases and then decreases with increasing the Cu^{2+} concentration in the slurry, which is still significantly higher than that of single $Cu(NO_3)_2$. Results show that the reaction between $Cu(NO_3)_2$ and H_2O_2 produces strong oxidizing substances, which contributes to the increase of the oxidation rate. However, excessive $Cu(NO_3)_2$ can prevent the oxidation of W. In addition, it is observed that the binding energy of W^{6+} in the conditions using the mixed-oxidant slurries appear the same leftward shift, indicating that the surfaces of the samples contain remaining soluble W^{6+}. This is consistent with the dissolution of WO_3 on the W surface under alkaline conditions, as proposed by HEUMANN and STOLICA [25].

The polarization curves of W samples in different slurries were also measured, and the corrosion potential (φ_{corr}) and corrosion current density (J_{corr}) under different conditions were calculated by the Tafel method, as shown in Fig. 8. The addition of H_2O_2 and $Cu(NO_3)_2$ increases the

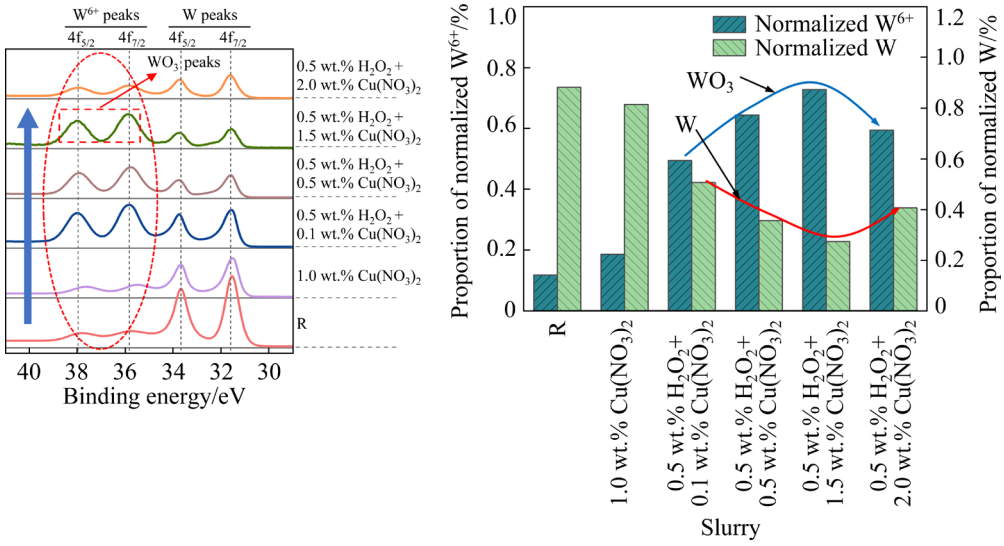

Fig. 7 XPS results of treated W surfaces after soaking by different slurries: (a) XPS spectra; (b) Fitting peak proportions of W and W^{6+}

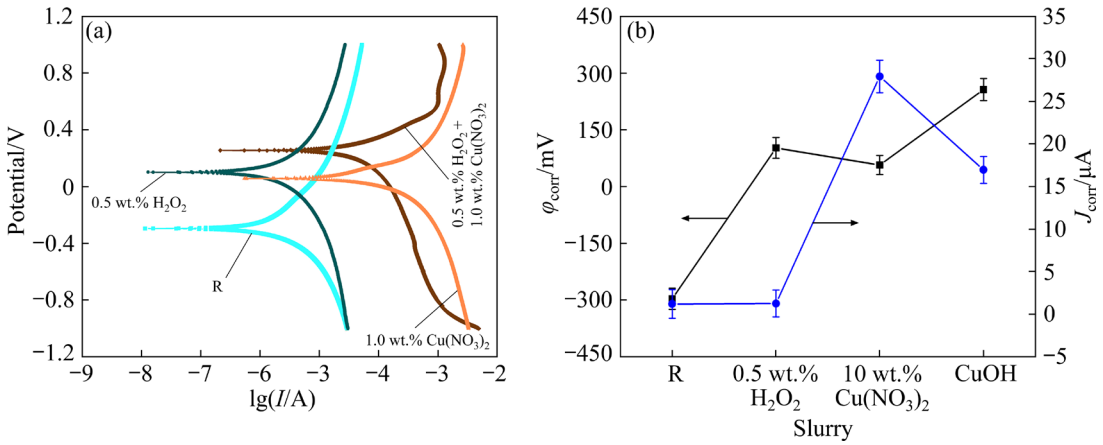

Fig. 8 Potentiodynamic results under various oxidant conditions: (a) Polarization curves; (b) φ_{corr} and J_{corr} curves

φ_{corr} and improves the overall corrosion resistance of W. However, under the condition using mixed oxidants, φ_{corr} increases by more than 300 mV, which might be due to the formation of a WO_3 passivation layer (confirmed by XPS data). The difference in φ_{corr} suggests the formation of different oxides when using different oxidants, leading to variations in the oxidation rate.

In general, J_{corr} tends to increase with the ion concentration in the slurry. However, under the condition with mixed oxidants, J_{corr} first decreases and then increases with increasing $Cu(NO_3)_2$ concentration, as given in Table 2. Results reveal that the reaction between $Cu(NO_3)_2$ and H_2O_2 is conducive to the formation of oxide passivation layer. However, excessive Cu^{2+} adsorption on the W surface slows down the oxidation reaction, consequently enhancing the corrosion rate of the W surface.

Table 2 Dynamic potential polarization results of slurries with different catalyst concentrations

Slurry	φ_{corr}/mV	J_{corr}/μA
0.5 wt.% H_2O_2 + 0.1 wt.% $Cu(NO_3)_2$	213.30	29.77
0.5 wt.% H_2O_2 + 0.5 wt.% $Cu(NO_3)_2$	224.21	28.81
0.5 wt.% H_2O_2 + 1.0 wt.% $Cu(NO_3)_2$	256.31	16.95
0.5 wt.% H_2O_2 + 1.5 wt.% $Cu(NO_3)_2$	327.70	22.39
0.5 wt.% H_2O_2 + 2.0 wt.% $Cu(NO_3)_2$	333.14	24.93

The reactivity between H_2O_2 and Cu^{2+} is higher than that of Fe^{3+}–H_2O_2 reaction [26]. The final product of the Fenton-like reaction is ·OH, which can oxidize W efficiently. Therefore, it is necessary to validate the existence and quantity of ·OH produced in the Fenton-like reaction. PNDA can be easily oxidized by ·OH and thus suitable for quantitative measurement of ·OH production [16,27]. The PNDA combines with ·OH to form ·OH — PNDA, which results in a decreased absorption peak at 440 nm. In this study, the intensity of the absorption peak of pure PNDA reaches 3.700 near 440 nm, as shown in Fig. 9. Compared with the single H_2O_2 and $Cu(NO_3)_2$ slurry, the group with mixed oxidants shows the reduced absorption peak intensity, indicating the presence of ·OH in the mixed oxidant slurry. This also indirectly verifies the Fenton-like reaction between $Cu(NO_3)_2$ and H_2O_2.

Figure 10 shows the changes in the intensity of PNDA absorption peak at about 440 nm for various slurries with different concentrations of $Cu(NO_3)_2$.

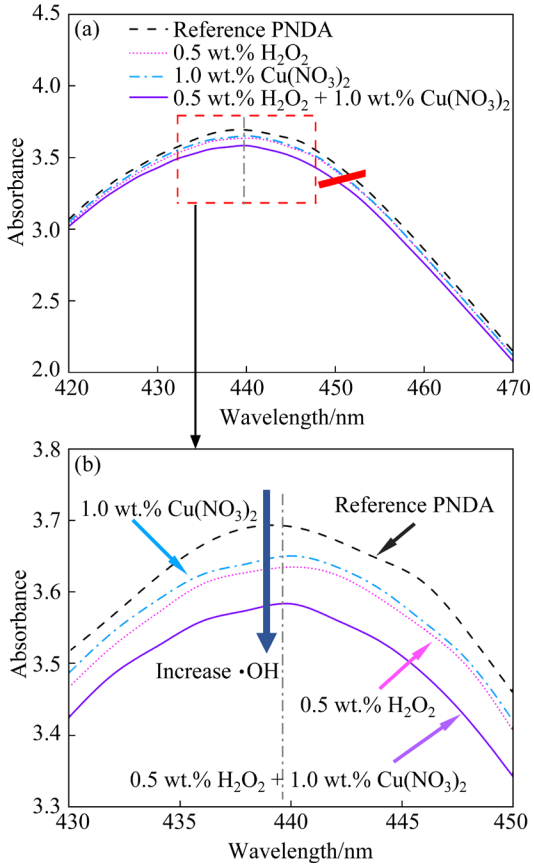

Fig. 9 UV-visible spectra of pure PNDA and its solution added with various oxidants

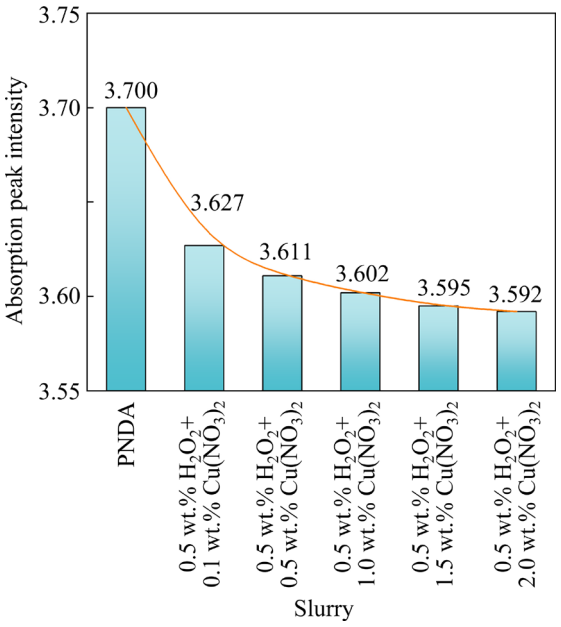

Fig. 10 Changes in intensity of PNDA absorption peak at about 440 nm for various slurries with different concentrations of $Cu(NO_3)_2$

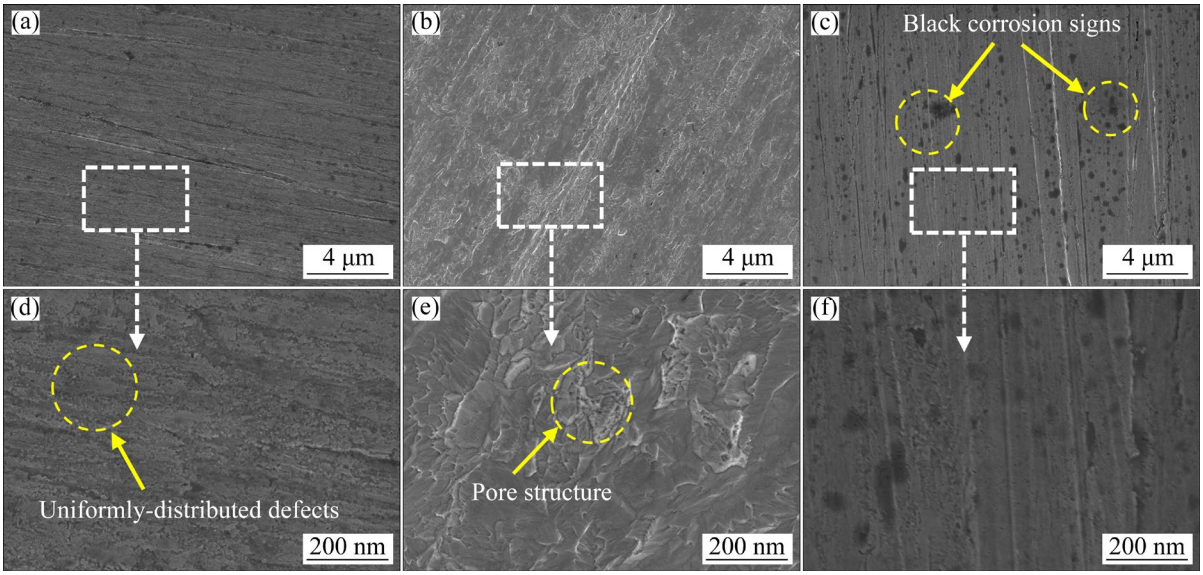

Fig. 11 SEM images of W surfaces corroded with different slurries: (a, d) 1.0 wt.% $Cu(NO_3)_2$; (b, e) 0.5 wt.% H_2O_2; (c, f) 0.5 wt.% H_2O_2 + 1.0 wt.% $Cu(NO_3)_2$

In this experiment, the concentration of H_2O_2 was maintained at 0.5 wt.%. It is seen that the absorption peak intensity near 440 nm is greatly reduced after the addition of mixed oxidants. The declining rate of absorption peak intensity decreases with the increase of $Cu(NO_3)_2$ concentration. When $Cu(NO_3)_2$ concentration increases from 1.5 to 2.0 wt.%, the absorption peak intensity decreases by only 0.003. Regarding the results shown in Figs. 5 and 6, it can be concluded that the mixed oxidants of $Cu(NO_3)_2$ and H_2O_2 ensures a better surface quality with high MRR due to the generation of sufficient amount of ·OH, while excessive $Cu(NO_3)_2$ may accelerate the consumption of H_2O_2 and then results in an insufficient supply of ·OH.

3.3 Effect of slurry composition on surface morphology

Figure 11 presents the SEM images of W surfaces corroded with different slurries for 30 min. After corrosion test with $Cu(NO_3)_2$, uniform corrosion defects are observed on the surface of W sample, (Figs. 11(a, d)); while after corrosion test with H_2O_2, defects are replaced by etch pit, as shown in Figs. 11(b, e). The oxidation efficiency of single $Cu(NO_3)_2$ is poor and there exists many corrosion defects on the surface, but porous oxide layers can be formed on the W surface under the action of H_2O_2. In contrast, the surface morphology of W treated with mixed oxidant slurry show the combined characteristics obtained under the action of single H_2O_2 and $Cu(NO_3)_2$, along with black spots. The EDS characterization (Fig. 12) confirms that the predominant elements in black spots are W and O, which results from the corrosion of WO_3 by OH^-. This also indicates that the oxide layer formed using the H_2O_2 slurry is not WO_3, since there is no sign of black spots on the sample surface.

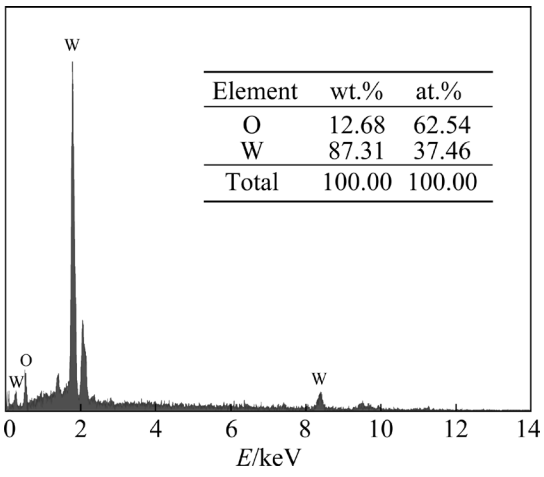

Element	wt.%	at.%
O	12.68	62.54
W	87.31	37.46
Total	100.00	100.00

Fig. 12 EDS analysis result of black spot

The morphologies of W surfaces before and after CMP process using different slurries are shown in Fig. 13. It is seen that the surface of the original W sample exhibits rough and uneven characteristics, featuring numerous holes of varying sizes (Figs. 13(a, e)). After processing with

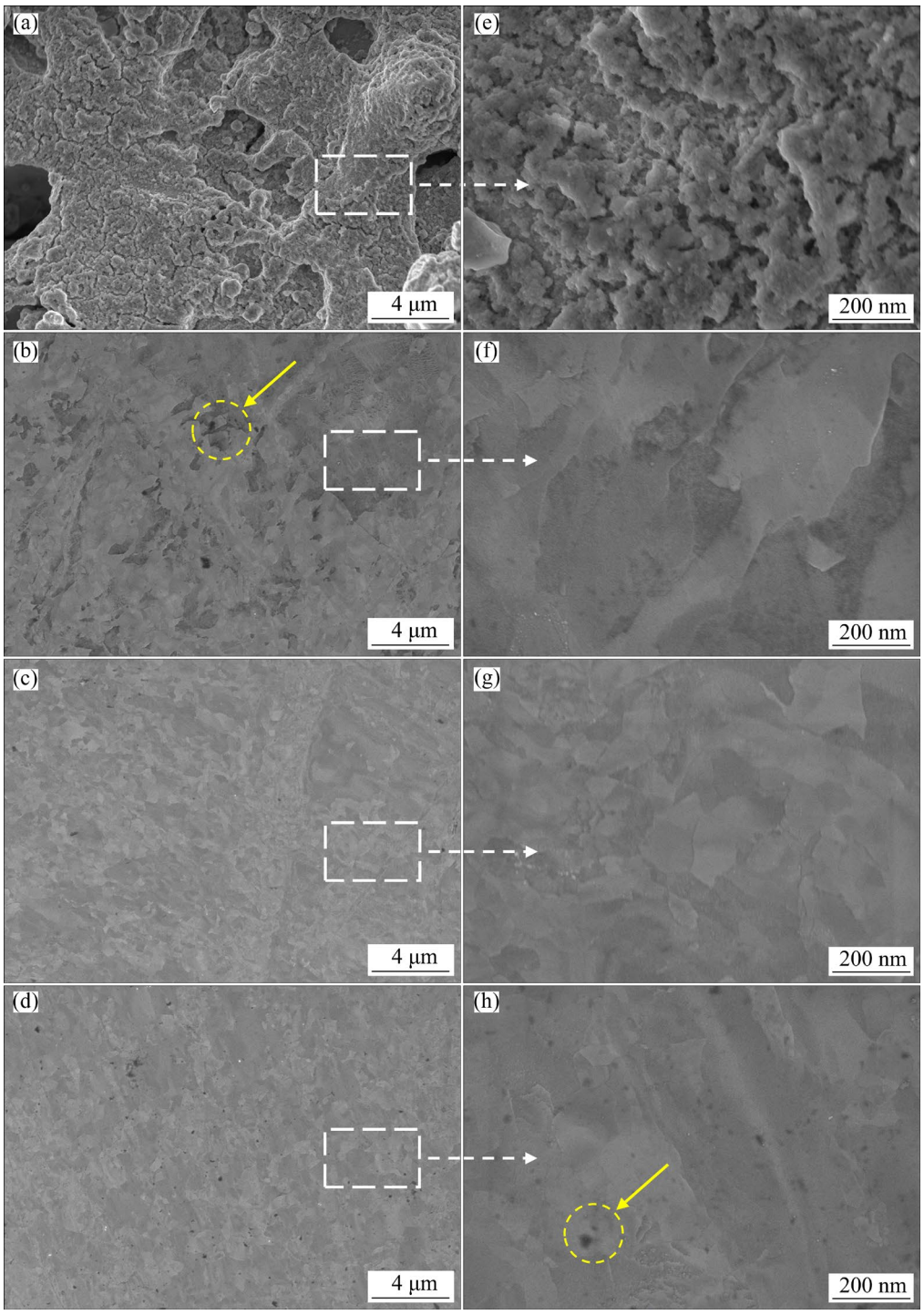

Fig. 13 SEM surface morphologies of original W sample (a, e), and CMP-W surfaces using H_2O_2 (b, f), $Cu(NO_3)_2$ (c, g), and H_2O_2+$Cu(NO_3)_2$ (d, h) slurries

H_2O_2 slurry, the surface of W exhibits evident grain boundary-like morphologies and pore structures, which may be attributed to uneven corrosion (Figs. 13(b, f)). By using $Cu(NO_3)_2$ slurry, some uniform corrosion defects are maintained on the W surface after CMP processing, as shown in Figs. 13(c, g). After processing with a mixed oxidant slurry, the surface of W shows a combined morphology of grain boundary-like feature and corrosion defects (Figs. 13(d, h)). The presence of the former can be attributed to the chemical coupling corrosion between W and H_2O_2, which primarily occurs at the grain boundaries. In comparison, it is suggested that the higher surface

uniformity should correspond to the greater oxidation rate when subjected to a mixed oxidant. Therefore, controlling the concentration of the oxidant and the processing time is beneficial to improving surface quality and mitigating the occurrence of surface defects.

3.4 Fenton-like reaction and material removal mechanism

On the basis of the Fenton reaction process, the step reactions between Cu^{2+} and H_2O_2, which produces the strong oxidizing ·OH, can be proposed as follows:

$$Cu^{2+}+H_2O_2 \overset{K_I}{\rightleftharpoons} CuOOH^{+}+H^{+} \quad (5)$$

$$CuOOH^{+}+H_2O_2 \underset{\text{Slow}}{\overset{K_I}{\rightleftharpoons}} CuOH^{2+}+H_2O+O_2^{-} \quad (6)$$

$$CuOH^{2+}+H_2O_2 \rightarrow Cu^{2+}+H_3O^{+}+O_2^{-} \quad (7)$$

$$O_2^{-}+Cu^{2+} \rightarrow CuOO^{+} \quad (8)$$

$$CuOO^{+} \xrightarrow{K_{III}} Cu^{+}+O_2 \quad (9)$$

$$Cu^{+}+H_2O_2 \rightarrow Cu^{2+}+OH^{-}+\cdot OH \quad (10)$$

$$\cdot OH+H_2O_2 \rightarrow H_3O^{+}+O_2^{-} \quad (11)$$

As shown in Fig. 14, a schematic illustration of the Cu^{2+}/H_2O_2 Fenton-like reaction mechanism is proposed. First, $CuOOH^{+}$ is formed in the reversible reaction (Eq. (5)). In the slow step (Eq. (6)), the O—O bond of $CuOOH^{+}$ reacts with the second H_2O_2 molecule to generate the superoxide radical ion O_2^{-}. Then, $CuOH^{2+}$ reacts with H_2O_2 (Eq. (7)) to generate O_2^{-}, which then coordinates with Cu^{2+} to form the superoxide copper(II) ion $CuOO^{+}$. The formation of Cu^{+} proposed in Eq. (9) is similar to that of the known superoxochromium(III) ion $CrOO^{+}$ [28]. Cu^{+} continues to react with H_2O_2 in a Fenton-like reaction to produce ·OH (Eq. (10)). The generated ·OH can react with excess H_2O_2 to generate O_2^{-} (Eq. (11)). Equations (8)−(11) thus result in a cycle reaction chain for decomposition of H_2O_2, as introduced by BAKAC et al [29].

Based on the above reaction mechanism, the material removal mechanism of W can be proposed, as shown in Fig. 15. In alkaline slurry without oxidant, the formation rate of the WO_3 passivation layer is low. The material removal depends on the chemical dissolution of WO_3 by OH^{-} to form WO_4^{2-}, and hence the MRR is limited. The oxide layer formed in H_2O_2 slurry is thicker, but the formation of the hard WO_x ($0<x<3$) layer limits the mechanical wear removal rate. The increased MRR is actually due to the high solubility of the generated $H_2W_3O_{12}$, which accelerates the chemical removal rate of W. When subjected to the mixed oxidant slurry, the bulk W surface can be oxidized by ·OH and O_2 to form soft WO_3 passivation layer. Such oxide layer can be readily removed by mechanical wear, and also prevent further corrosion of the substrate. Thus, both MRR and surface quality are significantly enhanced.

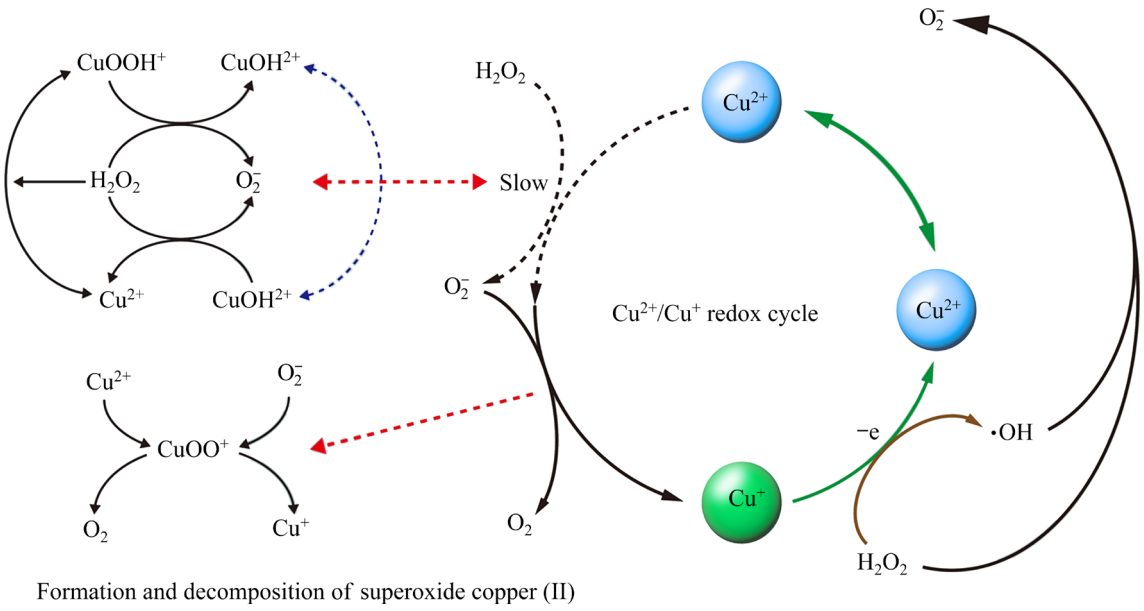

Fig. 14 Schematic illustration of Cu^{2+} and H_2O_2 Fenton-like reaction mechanism

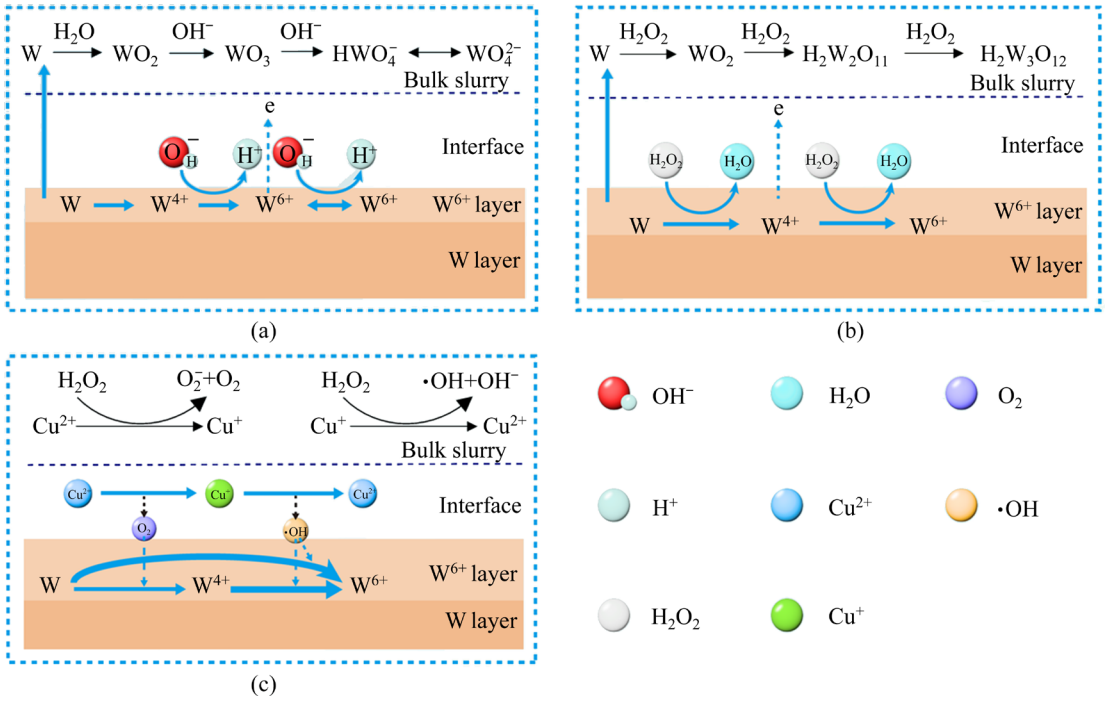

Fig. 15 Reaction mechanism of W oxidation in different slurry systems: (a) R (pH=9); (b) H_2O_2; (c) H_2O_2+$Cu(NO_3)_2$

4 Conclusions

(1) Compared to the single oxidant such as $Cu(NO_3)_2$ or H_2O_2, the strong oxidizing ·OH formed by the Fenton-like reaction in mixed oxidants can significantly convert W into a soft passive layer with lower hardness, making the mechanical removal of W more easily, which is the reason for the high polishing rate.

(2) The MRR and SER have significantly different dependencies on the change in $Cu(NO_3)_2$ concentration, which is related to the excessive consumption of H_2O_2 and the rapid supply of excessive Cu^{2+} to the surface to prevent the oxidation of W.

(3) The rapid formation and removal of the WO_3 layer mainly affect the polishing efficiency and surface quality of W-CMP. It is found that the optimal oxidant for achieving the balance is the mixture of 0.5 wt. %H_2O_2 + 1.0 wt.% $Cu(NO_3)_2$.

CRediT authorship contribution statement

Hong-yu CHEN: Data curation, Supervision, Project administration, Funding acquisition, Writing − Review & editing; **Lin WANG:** Conceptualization, Methodology, Writing − Original draft, Writing − Review & editing; **Feng PENG:** Visualization; **Meng-meng SHEN:** Software; **Wei HANG:** Writing − Review & editing, Funding; **Tufa Habtamu BERI:** Visualization; **Hui-bin ZHANG:** Writing − Review & editing, Supervision, Funding; **Jun ZHAO:** Formal analysis; **Yun-xiao HAN:** Validation; **Bing-hai LYU:** Writing − Review & editing.

Declaration of competing interest

The authors declare that they have no known competing financial interests or personal relationships that could have appeared to influence the work reported in this paper.

Acknowledgments

This work is supported by the National Natural Science Foundation of China (No. 52275467), the National Key Research and Development Program of China (No. 2023YFE0202900), the Natural Science Foundation of Zhejiang Province, China (No. LZY23E050004), and the Fundamental Research Funds for the Provincial Universities of Zhejiang Province, China (No. RF-A2022002).

References

[1] CHEN Hong-yu, XU Qiu, WANG Jia-huan, LI Peng, YUAN Ju-long, LYU Bing-hai, WANG Jin-hu, TOKUNAGA K, YAO Gang, LUO Lai-ma, WU Yu-cheng. Effect of surface quality on hydrogen/helium irradiation behavior in tungsten

[J]. Nuclear Engineering and Technology, 2022, 54(6): 1947−1953.

[2] ZHAO Jun, XIANG Yong-chao, FAN Cheng. A new method for polishing the inner wall of a circular tube with a soft abrasive rotating jet [J]. Powder Technology, 2022, 398: 117068.

[3] FAN Rong-lei, WU Yong, CHEN Ming-he, XIE Lan-sheng. Relationship among microstructure, mechanical properties and texture of TA32 titanium alloy sheets during hot tensile deformation [J]. Transactions of Nonferrous Metals Society of China, 2020, 30(4): 928−943.

[4] ZENG Min, YAN Hong, YU Bao-biao, HU Zhi. Microstructure, microhardness and corrosion resistance of laser cladding Ni−WC coating on AlSi5Cu1Mg alloy [J]. Transactions of Nonferrous Metals Society of China, 2021, 31(9): 2716−2728.

[5] YANG Jun-jun, CHEN Gang, CHEN Zheng, MU Xiao-dong, YU Ying, ZHANG Lin, LI Xing-yu, QU Xuan-hui, QIN Ming-li. Effects of doping route on microstructure and mechanical properties of W−1.0wt.%La_2O_3 alloys [J]. Transactions of Nonferrous Metals Society of China, 2020, 30(12): 3296−3306.

[6] DA SILVA E N, DOS SANTOS A A A, DO NASCIMENTO R M, ALVES S M, GUIMARAES R D, FILGUEIRA M. Investigation of characteristics and properties of spark plasma sintered ultrafine WC−6.4Fe3.6Ni alloy as potential alternative WC-Co hard metals [J]. International Journal of Refractory Metals and Hard Materials, 2021, 101: 105669.

[7] ZHANG Rui-ying, JIANG Fan, CHEN Shu-jun. Comparison of energy acted on workpiece among twin-body plasma arc welding, non-transferred plasma arc welding and plasma arc welding [J]. Journal of Manufacturing Processes, 2016, 24: 152−160.

[8] XU Liang, CHEN Hong-yu, LYU Bing-hai, HANG Wei, YUAN Ju-long. Study on rheological properties and polishing performance of viscoelastic material for dilatancy pad [J]. Precision Engineering, 2022, 77: 328−339.

[9] WANG Ze-chun, CHEN Shi-yao, YANG Sheng-lan, LUO Qun, JIN Yan-cheng, XIE Wei, ZHANG Li-jun, LI Qian. Light-weight refractory high-entropy alloys: A comprehensive review [J]. Journal of Materials Science & Technology, 2023, 151: 41−65.

[10] ABEDINI B, PARVINI AHMADI N, YAZDANI S, MAGAGNIN L. Electrodeposition and corrosion behavior of Zn−Ni−Mn alloy coatings deposited from alkaline solution [J]. Transactions of Nonferrous Metals Society of China, 2020, 30(2): 548−558.

[11] LI Zhe-xuan, BAO Ya-ting, WU Lian-kui, CAO Fa-he. Oxidation and tribological properties of anodized Ti45Al8.5Nb alloy [J]. Transactions of Nonferrous Metals Society of China, 2021, 31(11): 3439−3451.

[12] LI Geng-zhuo, XIAO Chen, ZHANG Shi-bo, SUN Ruo-yu, WU Yong-bo. An experimental investigation of silicon wafer thinning by sequentially using constant-pressure diamond grinding and fixed-abrasive chemical mechanical polishing [J]. Journal of Materials Processing Technology, 2022, 301: 117453.

[13] QI Huan, WANG Yue-lei, QI Zi-jian, SHI Li-wu, FANG Zhu-fang, ZHANG Li, RIEMER O, KARPUSCHEWSKI B. A novel grain-based DEM model for evaluating surface integrity in scratching of RB-SiC ceramics [J]. Materials, 2022, 15(23): 8486.

[14] YE Meng-chao, DING Ting-ting, ZHOU Hao, HE Feng-jiao. Nucleation and growth mechanism of electrodeposited Ni−W alloy [J]. Transactions of Nonferrous Metals Society of China, 2021, 31(6): 1842−1852.

[15] CHENG Zhi-chao, QIN Shi-kang, FANG Zhu-fang. Numerical modeling and experimental study on the material removal process using ultrasonic vibration-assisted abrasive water jet [J]. Frontiers in Materials, 2022, 9: 895271.

[16] PODDAR M K, RYU H Y, YERRIBOINA N P, JEONG Y A, LEE J H, KIM T G, KIM J H, PARK J D, LEE M G, PARK C Y, HAN S J, CHOI J G, PARK J G. Nanocatalyst-induced hydroxyl radical ((OH)—O-center dot) slurry for tungsten CMP for next-generation semiconductor processing [J]. Journal of Materials Science, 2020, 55(8): 3450−3461.

[17] LIM J H, PARK J H, PARK J G. Effect of potassium ferricyanide in the acid solution on performance of tungsten chemical mechanical planarization [J]. Journal of the Electrochemical Society, 2012, 159(4): 363−366.

[18] LIM J H, PARK J H, PARK J G. Effect of iron(III) nitrate concentration on tungsten chemical-mechanical-planarization performance [J]. Applied Surface Science, 2013, 282: 512−517.

[19] ZHOU Kun, XU Jia-yu, XIAO Gui-jian, HUANG Yun. A novel low-damage and low-abrasive wear processing method of C_f/SiC ceramic matrix composites: Laser-induced ablation-assisted grinding [J]. Journal of Materials Processing Technology, 2022, 302: 117503.

[20] KIM K, LEE K, SO S, CHO S, LEE M, YOU K, MOON J, SONG T. Fenton-like reaction between copper ions and hydrogen peroxide for high removal rate of tungsten in chemical mechanical planarization [J]. ECS Journal of Solid State Science and Technology, 2018, 7(3): 91−95.

[21] CHEN Hong-yu, WANG Lin, PENG Feng, XU Qiu, XIONG Yao-xu, ZHAO Shi-jun, TOKUNAGA K, WU Zheng-gang, MA Yi, CHEN Peng-qi, LUO Lai-ma, WU Yu-cheng. Hydrogen retention and affecting factors in rolled tungsten: Thermal desorption spectra and molecular dynamics simulations [J]. International Journal of Hydrogen Energy, 2023, 48(78), 30522−30531.

[22] PODDAR M K, JALALZAI P, SAHIR S, YERRIBOINA N P, KIM T G, PARK J G. Tungsten passivation layer (WO_3) formation mechanisms during chemical mechanical planarization in the presence of oxidizers [J]. Applied Surface Science, 2021, 537: 147862.

[23] XU Liang, WANG Lin, CHEN Hong-yu, WANG Xu, CHEN Fang-yuan, LYU Bing-hai, HANG Wei, ZHAO Wen-hong, YUAN Ju-long. Effects of pH values and H_2O_2 concentrations on the chemical enhanced shear dilatancy polishing of tungsten [J]. Micromachines, 2022, 13(5): 762.

[24] KNEER E A, RAGHUNATH C, MATHEW V, RAGHAVAN S, JEON J S. Electrochemical measurements during the chemical mechanical polishing of tungsten thin films [J]. Journal of the Electrochemical Society, 1997, 144(9): 3041−3049.

[25] HEUMANN T, STOLICA N. The electrochemical behaviour of tungsten-I. The dissolution of tungsten and tungsten

oxides in buffer solutions [J]. Electrochimica Acta, 1971, 16(5): 643−651.

[26] GUO Jiang, SHI Xiao-lin, SONG Chuan-ping, NIU Lin, CUI Hai-long, GUO Xiao-guang, TONG Zhen, YU Nan, JIN Zhu-ji, KANG Ren-ke. Theoretical and experimental investigation of chemical mechanical polishing of W−Ni−Fe alloy [J]. International Journal of Extreme Manufacturing, 2021, 3(2): 025103.

[27] WANG Lin, PENG Feng, CHEN Hong-yu, HANG Wei, YU Cui-ping, CHEN Shun-hua, ZHAO Shi-jun, WU Zheng-gang, MA Yi, LYU Bing-hai, YUAN Ju-long. The influence of pH and H_2O_2 on surface quality and material removal rate during W-CMP [J]. The International Journal of Advanced Manufacturing Technology, 2023, 127: 4097−4110.

[28] PEREZ-BENITO J F, ARIAS C. Kinetics and mechanism of the reactions of superoxochromium(III) ion with biological thiols [J]. The Journal of Physical Chemistry A, 1998, 102(29): 5837−5845.

[29] BAKAC A, WON T J, ESPENSON J H. Novel pathways in the reactions of superoxometal complexes [J]. Inorganic Chemistry, 1996, 35(8): 2171−2175.

Cu^{2+}和 H_2O_2 类芬顿反应促进钨的高效化学机械抛光

陈泓谕[1,2]，王 林[1]，彭 枫[1]，沈蒙蒙[1]，杭 伟[1,2]，
Tufa Habtamu BERI[3]，张惠斌[4]，赵 军[1,2]，韩云晓[1,2]，吕冰海[1,2]

1. 浙江工业大学 机械工程学院，杭州 310023；
2. 浙江工业大学 特种装备制造与先进加工技术教育部重点实验室，杭州 310023；
3. Adama Science and Technology University, Adama 1888, Ethiopia;
4. 浙江工业大学 材料科学与工程学院，杭州 310014

摘 要：将 Cu^{2+}和 H_2O_2 类芬顿反应应用于化学机械抛光中，以实现钨的高效高质量加工。采用扫描电子显微镜、X 射线光电子能谱、紫外−可见分光光度计和电化学实验等方法研究了钨在抛光过程中的显微组织演变和材料去除率，讨论了钝化行为和材料去除机理。结果表明，与单一氧化剂 H_2O_2 或 $Cu(NO_3)_2$ 相比，使用混合氧化剂 H_2O_2+$Cu(NO_3)_2$ 可以获得更高的抛光效率和表面质量。材料去除率的提高归因于基体与类芬顿反应产生的羟基自由基之间的化学反应将钨快速氧化成 WO_3。此外，材料去除率和静态腐蚀速率对 $Cu(NO_3)_2$ 浓度的变化表现出明显不同的依赖性，而实现抛光效率和表面质量平衡的最佳氧化剂为 0.5%H_2O_2+1.0%$Cu(NO_3)_2$(质量分数)。

关键词：化学机械抛光；钨；类芬顿反应；羟基自由基；材料去除机理

(Edited by Bing YANG)